Archive of Applied Mechanics 72 (2002) 171–188 © Springer-Verlag 2002
DOI 10.1007/s00419-002-0202-4

A classification of higher-order strain-gradient models – linear analysis

H. Askes, A. S. J. Suiker, L. J. Sluys

Summary The use of higher-order strain-gradient models in mechanics is studied. First, existing second-gradient models from the literature are investigated analytically. In general, two classes of second-order strain-gradient models can be distinguished: one class of models has a direct link with the underlying microstructure, but reveals instability for deformation patterns of a relatively short wave length, while the other class of models does not have a direct link with the microstructure, but stability is unconditionally guaranteed. To combine the advantageous properties of the two classes of second-gradient models, a new, fourth-order strain-gradient model, which is unconditionally stable, is derived from a discrete microstructure. The fourth-gradient model and the second-gradient models are compared under static and dynamic loading conditions. A numerical approach is followed, whereby the element-free Galerkin method is used. For the second-gradient model that has been derived from the microstructure, it is found that the model becomes unstable for a limited number of wave lengths, while in dynamics, instabilities are encountered for all shorter wave lengths. Contrarily, the second-gradient model without a direct link to the microstructure behaves in a stable manner, although physically unrealistic results are obtained in dynamics. The fourth-gradient model, with a microstructural basis, gives stable and realistic results in statics as well as in dynamics.

Keywords Strain-gradient Models, Higher-order Continuum, Microstructure, Wave Propagation, Stability

1 Introduction

Classical continuum theories assume that the stresses in a material point depend only on the first-order derivative of the displacements, i.e. on the strains, and not on higher-order displacement derivatives. As a consequence of this limitation on the kinematic field, a classical continuum is not always capable of adequately describing heterogeneous phenomena. For instance, unrealistic singularities in the stress and/or strain field may occur nearby imperfections. Furthermore, severe problems in the simulation of localisation phenomena with classical continua have been encountered, such as loss of well-posedness in the mathematical description and pathological mesh-dependence in numerical simulations (see [25] for an overview). To avoid these types of deficiencies, it has been proposed to include higher-order strain gradients into the constitutive equations, so that the defects of the classical continuum may be successfully overcome, [4, 12, 17, 19, 22, 24, 25]. The second-order strain gradients that are normally used for these purposes introduce accessory material parameters that reflect the microstructural properties of the material. However, the second-gradient term is often *postulated,* rather than *derived from the microstructure.* Hence, this class of models can be denoted as phenomenological.

Received 13 June 2001; accepted for publication 6 November 2001

H. Askes (✉), L. J. Sluys
Koiter Institute Delft/Delft University of Technology,
Faculty of Civil Engineering and Geosciences,
P.O. Box 5048, NL-2600 GA Delft, The Netherlands
e-mail: H.Askes@CiTG.tudelft.nl

A. S. J. Suiker
Koiter Institute Delft/Delft University of Technology,
Faculty of Aerospace Engineering, P.O. Box 5058,
NL-2600 GB Delft, The Netherlands

Another class of problems in which the use of classical continua fails and in which higher-order gradients are employed, is that where the characteristics of a *discrete* medium must be approximated. As an example of this class of problems, wave propagation through a granular medium can be considered. The dispersive properties that are predicted by a discrete material model and that have been found in experiments, are not obtained when a classical continuum model is used. The addition of higher-order gradients can improve the performance of the classical continuum in the sense that the dispersive behaviour of the discrete model is reproduced with a higher accuracy, [10, 18, 28–30]. This is a direct consequence of the procedure that is commonly used to enhance the classical continuum with higher-order gradients: homogenisation of the discrete medium may lead to higher-order gradients in a direct and straightforward manner.

If regularisation of singularities or discontinuities is required, higher-order gradients are used for *smoothing* the non-uniformity or singularities in the strain field. On the other hand, if a more accurate representation of the discrete microstructure is desired, the higher-order gradients are used to *introduce* a non-uniformity in the strain field. In Fig. 1, the two concepts of using higher-order gradients are illustrated.

The higher-order gradients that result from the different motivations to enhance the classical continuum can have opposite effects. As is detailed in Sec. 2, this can easily be substantiated when a linear elastic one-dimensional geometry is considered for either class of higher-order gradient models. Accordingly, it is demonstrated that the analytical solution may be either of the exponential type (smoothing heterogeneity) or of the harmonic type (introducing heterogeneity). Furthermore, energy considerations reveal the stability of the models.

In Sec. 3, a second-order strain-gradient model and a fourth-order strain-gradient model will be derived from a discrete microstructure. Also, another second-gradient model will be examined that belongs to the phenomenological class of higher-order gradient models. The derived fourth-gradient model holds a close relation with the discrete microstructure, as is illustrated via a dispersion analysis in Sec. 4. Moreover, the inclusion of the fourth-order gradient term mitigates some of the cumbersome aspects of the second-order gradient term. Finally, the two second-gradient models and the fourth-gradient model are tested in a linear static context (Sec. 5) and in a linear dynamic context (Sec. 6).

2
Classification of second strain gradient models

The higher-order strain-gradient models that exist in the literature in virtually all cases are concerned with second-order strain gradients; exceptions are Refs. [3, 24], where first-order gradients are used, and Refs. [6, 11, 28], in which also fourth-order gradients are included.

Regularising strain gradients have been used in elasticity, [4, 31–33], plasticity, [1, 12, 16, 17, 19, 25] and damage mechanics [6, 13, 21–23]. In these cases, the higher-order strain gradients have been postulated from a phenomenological point of view, either in the energy functional, [31], or directly in the constitutive relation, [16, 22]. For reasons of clarity, the restriction here is made to the one-dimensional case, combined with the linear elastic material behaviour. Following [2, 4], the enhanced constitutive relation can then be cast as

$$\sigma = E(\varepsilon - l^2\nabla^2\varepsilon) \ , \tag{1}$$

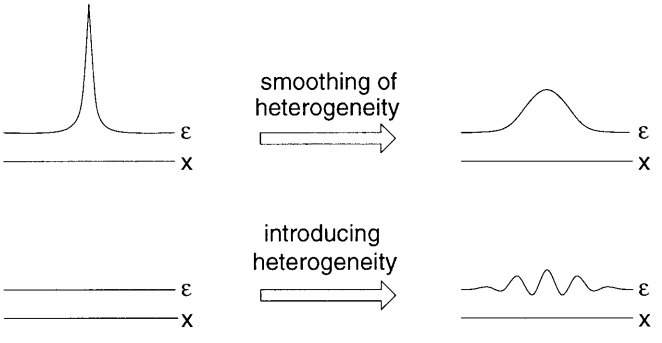

Fig. 1. Two motivations for using higher-order gradients: smoothing or regularisation of heterogeneities in the strain field (top) and the introduction of heterogeneities in the strain field (bottom)

where σ is the (axial) stress, E is the Young's modulus, ε is the (axial) strain and l is a material parameter with the dimension of length. The parameter l will be denoted as the *internal length scale*, as it reflects the micromechanical properties of the material. It is emphasized that micromechanical arguments can be given to incorporate higher-order strain gradients according to Eq. (1). However, to the authors' best knowledge, *no derivation of the higher-order terms from a micromechanical basis exists.*

Alternatively, strain gradients can be used to introduce heterogeneity into the continuum. As a result, the dispersive character of waves observed in experiments and in discrete material models can be simulated with a higher accuracy, [10, 18, 28–30]. By homogenising a discrete medium, a second-gradient model of the type

$$\sigma = E(\varepsilon + l^2 \nabla^2 \varepsilon) \ , \tag{2}$$

can be derived, see Sec. 3. In contrast to Eq. (1), the higher-order strain gradient term now appears with a positive sign.

2.1 Analytical solutions

The sign of the higher-gradient term completely determines the character of the higher-gradient model. This becomes manifest in the analytical solutions, which are obtained by combining the constitutive relations (1) or (2) with the uniaxial equilibrium equation $\partial\sigma/\partial x = 0$ (no body forces are considered) and the kinematic relation $\varepsilon = \partial u/\partial x$, with u denoting the longitudinal displacement of the one-dimensional medium. The use of Eq. (1) leads to an analytical solution for u of the form

$$u = A_1 + A_2 x + A_3 \ \exp(-x/l) + A_4 \exp(x/l) \ , \tag{3}$$

while using Eq. (2) results in

$$u = B_1 + B_2 x + B_3 \ \sin(x/l) + B_4 \ \cos(x/l) \ , \tag{4}$$

in which A_i and B_i are constants that have to be determined according to the boundary conditions. In either case, the response of the classical continuum is given by the constants A_1, A_2 and B_1, B_2, respectively. As can be seen, the sign of the second-gradient term determines whether the analytical solution is of the exponential type or of the harmonic type. An important difference between the two models is found when higher-order gradient activity is triggered by a local perturbation. For boundary-value problems, a local perturbation in Eq. (3) can lead to a *local* gradient activity in the strain field, while a local perturbation in Eq. (4) leads to a gradient activity in the *entire* domain. This is treated in more detail in Sec. 5.

2.2 Uniqueness

Following [4], the uniqueness of the static analytical solution is investigated next. To this end, it is assumed that two different solutions u_1 and u_2 exist that satisfy the equilibrium equation and the nonhomogeneous boundary conditions. For a proof of uniqueness, the difference between these two solutions $\Delta u = u_1 - u_2$ should vanish. This 'difference solution' should then satisfy the equilibrium equation and the *homogeneous* boundary conditions. A specimen of length L is considered, and the boundary conditions for the difference solution are taken as $\Delta u = 0$ and $\partial \Delta u/\partial x = 0$ both at $x = 0$ and at $x = L$.

First, Eq. (3) is considered. The four boundary conditions lead to the following system of equations:

$$\begin{aligned}
&A_1 + A_3 + A_4 = 0, \\
&A_1 + A_2 L + A_3 \ \exp(-L/l) + A_4 \ \exp(-L/l) = 0, \\
&A_2 + \frac{-A_3 + A_4}{l} = 0, \\
&A_2 + \frac{-A_3 \ \exp(-L/l) + A_4 \ \exp(L/l)}{l} = 0 \ .
\end{aligned} \tag{5}$$

By eliminating A_1 and A_2, a reduced coefficient matrix for A_3 and A_4 according to Eq. (1) can be determined. For finding a nontrivial solution for Δu (which corresponds to non-uniqueness) the determinant of this reduced coefficient matrix should vanish, i.e.

$$\mathrm{Det}\begin{bmatrix} \exp(-\alpha) - 1 + \alpha & \exp(\alpha) - 1 - \alpha \\ -\exp(-\alpha) + 1 & \exp(\alpha) - 1 \end{bmatrix} = 0 \ , \tag{6}$$

where $\alpha = L/l$. Since $\alpha > 0$, this leads to

$$f(\alpha) = (2 - \alpha)\exp(\alpha) + (2 + \alpha)\exp(-\alpha) - 4 = 0 \ . \tag{7}$$

It can be verified that for $\alpha \to 0$, both $f(\alpha)$ and its first derivative vanish. Furthermore, the second derivative of $f(\alpha)$ equals $-2\alpha\sinh(\alpha)$, which is negative for all $\alpha > 0$. Accordingly, $f(\alpha) < 0$ for all $\alpha > 0$, so that Eq. (7) can never be satisfied. Therefore, uniqueness is guaranteed for the model of Eq. (1).

A similar procedure can be followed to investigate the uniqueness of the solution according to Eq. (4). The determinant of the reduced coefficient matrix for B_3 and B_4 reads

$$\mathrm{Det}\begin{bmatrix} \sin(\alpha) - \alpha & \cos(\alpha) - 1 \\ \cos(\alpha) - 1 & -\sin(\alpha) \end{bmatrix} = 0 \ , \tag{8}$$

or

$$g(\alpha) = \alpha\sin(\alpha) + 2\cos(\alpha) - 2 = 0 \ , \tag{9}$$

which is satisfied when $\alpha = 2\pi m$ with m an arbitrary integer. Thus, uniqueness cannot be guaranteed for the model of Eq. (2) in the case $\alpha = L/l = 2\pi m$.

Remark 1. The same results have been obtained in [4] by a somewhat different procedure.

Remark 2. In the above procedure, the higher-order boundary conditions are taken as prescribed values for the first derivative of the displacement. The use of different higher-order boundary conditions leads to different considerations with respect to uniqueness. Taking prescribed second-order derivatives of the displacement can also lead to nonunique solutions with the model of Eq. (4). Although not shown here, in this case the values of α for which nonunique solutions are obtained coincide with those obtained via Eq. (9).

2.3
Energy considerations

The stability of the models of Eqs. (1) and (2) is studied by means of the potential energy density $\mathscr{U}$, given by

$$\mathscr{U} = \int_{\varepsilon} \sigma \mathrm{d}\varepsilon \ . \tag{10}$$

Substitution of the constitutive equations (1) and (2), integrating the higher-order terms by parts, and carrying out the integration results in

$$\mathscr{U} = \frac{1}{2}E\left(\varepsilon^2 + l^2\left(\frac{\partial\varepsilon}{\partial x}\right)^2\right) \ , \tag{11}$$

for the model of Eq. (1) and in

$$\mathscr{U} = \frac{1}{2}E\left(\varepsilon^2 - l^2\left(\frac{\partial\varepsilon}{\partial x}\right)^2\right) \ , \tag{12}$$

for the model of Eq. (2). In the derivation procedure above, the boundary integrals are assumed to vanish. Again, the only difference between the two models concerns with the sign of the higher-order term. However, this has severe implications for the stability of the model: positive terms have a stabilising effect on the overall response, while negative terms are destabilising. Thus, the model according to Eq. (1) is unconditionally stable, while the model of Eq. (2) may become unstable.

2.4 Comparison

The main characteristics of the two types of second-order strain-gradient models are summarised below. The behaviour of the second-gradient model with the negative sign in front of the higher-order term has better properties from the point of view of stability and uniqueness. However, the link with the underlying microstructure is less evident for this model. This becomes manifest in Sec. 4 when the dispersion relations of the two second-gradient models are studied and compared to the corresponding dispersion relation of a discrete medium. Indeed, the model with a positive sign in front of the higher-order term bears the closest relation with the discrete model. However, the use of this model in engineering practice is limited due to the possible emergence of nonuniqueness and instability, which may have a devastating effect on its response, e.g. [7, 27], see also Secs. 5 and 6.

The focus in the sequel of the paper is to consider a higher-order strain-gradient model that has the physical basis of the second-gradient model of Eq. (2), i.e. a close relationship with the underlying discrete medium, while the stability and uniqueness properties of the model according to Eq. (1) are also present. Thus, the aim is to consider a model that combines the advantageous properties of both types of second-gradient models.

3 Derivation of higher-order strain-gradient models from a discrete microstructure

In this section, higher-order strain gradient models are derived by means of homogenisation of the displacement field of a discrete model. In the discrete model, the particles are represented by individual masses. The inter-particle contacts are modelled via springs that connect the masses. For simplicity, it is assumed that all particles have the same spring stiffness K, particle mass M and inter-particle distance d. This geometry is depicted in Fig. 2 for which the equation of motion of particle n can be expressed as

$$M\ddot{u}_n + K(2u_n - u_{n+1} - u_{n-1}) = 0 \ , \tag{13}$$

where a superimposed dot denotes a time derivative. In the homogenisation procedure, it is assumed that the *continuous* displacement u equals the discrete displacement u_n at particle n. The displacement at the neighbouring particles is found by means of a Taylor series as

$$u(x \pm d) = u(x) \pm d\frac{\partial u(x)}{\partial x} + \frac{1}{2}d^2\frac{\partial^2 u(x)}{\partial x^2} \pm \frac{1}{6}d^3\frac{\partial^3 u(x)}{\partial x^3} + \frac{1}{24}d^4\frac{\partial^4 u(x)}{\partial x^4} + \cdots \ . \tag{14}$$

Next, the displacements of the discrete medium u_{n+1} and u_{n-1} are expressed in terms of the continuous displacement. These terms are substituted into Eq. (13). After division by the cross-sectional area of the medium A and the inter-particle distance d it is found that

$$\rho\ddot{u} = E\left(\frac{\partial^2 u}{\partial x^2} + \frac{1}{12}d^2\frac{\partial^4 u}{\partial x^4} + \frac{1}{360}d^4\frac{\partial^6 u}{\partial x^6} + \cdots\right) \ , \tag{15}$$

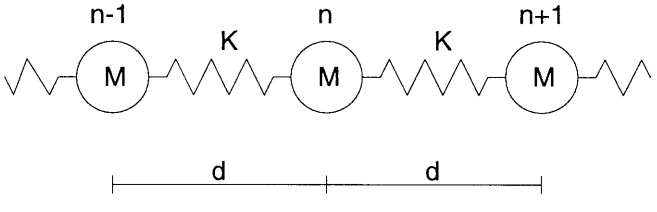

Fig. 2. Discrete medium – geometrical and mechanical properties

with the mass density $\rho = M/Ad$ and the Young's modulus $E = Kd/A$. Note that all odd derivatives of u have cancelled.

When the kinematic relation $\varepsilon = \partial u/\partial x$ is used, and the equation of motion of the continuum is expressed as $\rho\ddot{u} = \partial\sigma/\partial x$, the constitutive relation can be retrieved as

$$\sigma = E\left(\varepsilon + \frac{1}{12}d^2\frac{\partial^2\varepsilon}{\partial x^2} + \frac{1}{360}d^4\frac{\partial^4\varepsilon}{\partial x^4} + \cdots\right) \quad . \tag{16}$$

When Eq. (16) is truncated after the second-gradient term, a constitutive relation with the format of Eq. (2) is found, i.e. the second-gradient term is preceded by a *positive* sign, where $d = l\sqrt{12}$. Indeed, the above procedure illustrates the close relation between the discrete microstructure and the higher-order continuum according to Eq. (16).

As an alternative, it is possible to truncate Eq. (16) after the fourth-gradient term. Thus, a fourth-order strain-gradient model is obtained, [27, 28].

The homogenisation procedure as shown above unequivocally leads to a second-order strain-gradient term that is preceded by a positive sign, [10, 18, 28, 29]. Indeed, the second-gradient model with the negative sign, see Eq. (1), cannot be derived directly from a microstructure of discrete particles.

4
Dispersion analysis

As a first exploration of the performance of the various models, an analysis of dispersive waves is carried out. Dispersive behaviour of a medium is characterised by its ability to change the shape of propagating waves. In a mathematical context, this implies that the wave velocity must depend on the wave number.

To investigate the dispersive character of the discrete model of Eq. (13), the harmonic solution

$$u_n = \hat{u}\exp(\mathrm{i}k(ct - x_n))$$

is substituted, in which $\hat{u}$ is the amplitude, k is the wave number, c is the phase velocity, t is time and x_n is the coordinate of particle n. The wave number is related to the wave length λ via $\lambda k = 2\pi$. Using $x_n = nd, x_{n+1} = (n+1)d$ and $x_{n-1} = (n-1)d$, it is found that

$$\frac{Mk^2c^2}{K} = 4\sin^2\left(\frac{kd}{2}\right) \quad . \tag{17}$$

The angular frequency ω is defined as $\omega = ck$ and the elastic bar velocity is $c_e = \sqrt{E/\rho} = \sqrt{Kd^2/M}$. Consequently, the dispersion relation of the discrete medium can be expressed as

$$\frac{\omega}{c_e} = \frac{2}{d}\left|\sin\left(\frac{kd}{2}\right)\right| \quad . \tag{18}$$

A similar procedure is followed for the continuum models. Starting point is the one-dimensional equation of motion $\rho\ddot{u} = \partial\sigma/\partial x$, in which the various constitutive equations and the kinematic relation are substituted. In the resulting expression on the harmonic solution $u = \hat{u}\exp(\mathrm{i}k(ct - x))$ is substituted. For the second-gradient model with the negative sign, see Eq. (1), this results in

$$\frac{\omega}{c_e} = k\sqrt{1 + \frac{1}{12}k^2d^2} \quad , \tag{19}$$

with $d = l\sqrt{12}$. Since the second-order gradient model with a negative sign has not been derived from the discrete medium, the factor 1/12 is arbitrary. However, for a consistent comparison with the other models this factor has been adopted in the remainder of this study.

The dispersion relation for the second-gradient model with the positive sign (that is, the second-gradient truncation of Eq. (16)) reads

$$\frac{\omega}{c_e} = k\sqrt{1 - \frac{1}{12}k^2d^2} \quad , \tag{20}$$

and the dispersion relation for the fourth-gradient model taken from Eq. (16) can be elaborated as

$$\frac{\omega}{c_e} = k\sqrt{1 - \frac{1}{12}k^2d^2 + \frac{1}{360}k^4d^4} \quad . \tag{21}$$

In Fig. 3, the dispersion curves for the various models are plotted, taking $c_e = 1$ mm/s and $d = 1$ mm. For comparison also the dispersion relation of the classical continuum is plotted. While the classical continuum is nondispersive (the phase velocity $c = \omega/k$ is constant), the discrete medium and the higher-order strain gradient continua are dispersive. It can be seen that the second-gradient model with the positive sign and the fourth-gradient model give improved approximations of the discrete model, as compared to the classical continuum. On the other hand, the agreement between the second-gradient model with the negative sign and the discrete medium is poor.

However, the instability of the second-gradient model with the positive sign also becomes manifest in Fig. 3: for wave numbers larger than $\sqrt{12}/d$ the angular frequency and the phase velocity become imaginary, cf. Eq. (20). This means that waves with larger wave numbers (or, equivalently, with smaller wave lengths) cannot propagate through this medium. Instead, the imaginary frequency and velocity imply that the response occurs everywhere in the medium instantaneously. This is physically unrealistic. Therefore, these smaller wave lengths should not be considered. Filtering shorter waves occurs automatically in a *discrete* medium, where wave lengths smaller than two times the particle size cannot be monitored. However, in a *continuous* medium, all wave lengths can in principle be present. Especially when shock waves are investigated, all wave lengths are triggered by the loading. The imaginary angular frequency (or phase velocity) of these high-frequent waves prohibits a proper wave propagation simulation with this model, as will be illustrated in Sec. 6. The cut-off value for the wave number, i.e. the wave number for which the angular frequency is zero, dominates the static response of the second-gradient model with a positive sign. This cut-off value emerges at $k = \sqrt{12}/d$, cf. Fig. 3.

It must be emphasized that for the second-gradient model with the negative sign, as well as for the fourth-gradient model, a range of wave numbers exists for which the phase velocity is larger than the bar velocity of the classical continuum, for which a physical motivation is lacking. For the second-gradient model with the negative sign, this covers the *complete* range of wave numbers, while for the fourth-gradient model it only concerns the higher wave numbers, see Fig. 3. However, in the response of the fourth-gradient model the effect of these high-frequency waves are of minor importance, as will be demonstrated in Sec. 6.

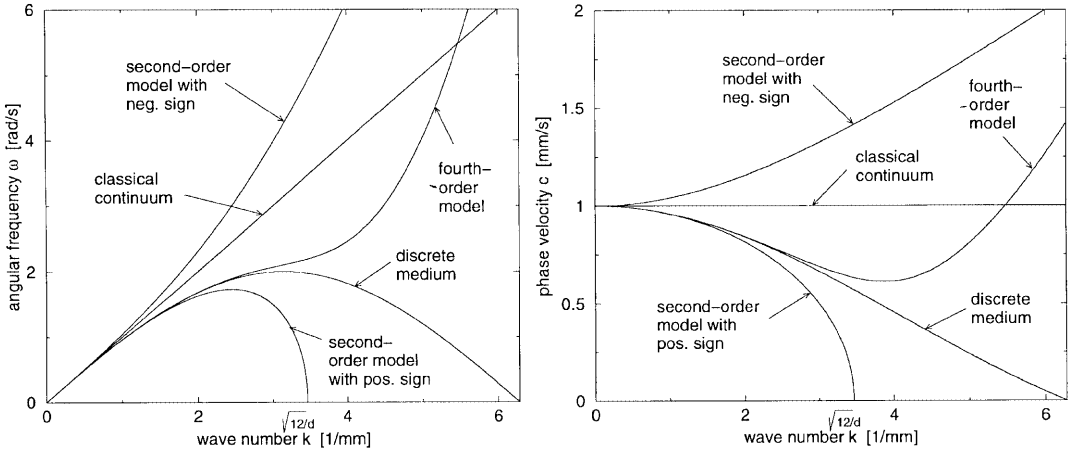

Fig. 3. Angular frequency versus wave number (left) and phase velocity versus wave number (right)

5
Linear static analysis

The higher-order gradient models are tested in a one-dimensional boundary value problem of which the geometry and the loading conditions are given in Fig. 4. An imperfection is placed in the centre of the bar to trigger higher-order gradient activity. Due to the presence of higher-order terms in the governing equations, additional boundary conditions are required. Following the literature, we impose zero values for the first-order spatial derivative of the strain at the boundaries in the second-gradient model, [6, 19, 22, 25]. Moreover, zero values for the third-order spatial derivative of the strain are imposed at the boundaries in the fourth-gradient model, [6]. The bar of Fig. 4 is subjected to an imposed displacement of 0.01 mm at its right end which corresponds to an average strain level of 0.001. The Young's modulus is taken as $E = 1000$ MPa.

Analytical solutions are available for the one-dimensional linear elastic case. However, in multi-dimensional cases numerical solution techniques are necessary. Therefore, the performance of the models is tested numerically. The problem has been solved by means of the element-free Galerkin (EFG) method, [8, 9]. This is a meshless discretisation method in which the shape functions can be formulated with an arbitrary order of continuity, which is advantageous when higher-order gradient models are investigated, [5, 6, 15, 20]. Discretisation aspects are treated in Appendix A. The bar of Fig. 4 has been discretised with 81 equally-spaced nodes and 400 equally-spaced integration points.

5.1
Second-gradient model with positive sign

The second-gradient model with the positive sign has been used, see Eq. (2), with $d = l\sqrt{12}$. For this model, the solution has a harmonic character, see Eq. (4). The number of wave lengths along the bar is $n = L/\lambda$, with L denoting the bar length and λ the wave length. The wave length is related to the wave number k via $\lambda = 2\pi/k$, while the critical wave number of the static case can be retrieved from the dispersion relation by requiring that the angular frequency (or the phase velocity) equals zero. This wave number equals $k = \sqrt{12}/d$, see Fig. 3. Thus, the number of wave lengths along the bar is given by

$$n = \frac{L\sqrt{12}}{2\pi d} \quad . \tag{22}$$

When this equation is compared to Eq. (9), and it is realised that $d = l\sqrt{12}$ for the current model, it can be seen that uniqueness fails in the case n from Eq. (22) equals the integer m. In Fig. 5, relation (22) is plotted for the problem in Fig. 4 where $L = 10$ mm. In this figure, especially these values of d are denoted for which n equals the integer m and, thus, for which uniqueness fails.

Remark 3. Note the difference between the wave number k and the number of wave lengths along the bar n. The wave number k denotes the number of wave lengths that fit into 2π, while n denotes the number of wave lengths that fit into the bar length L. More generally, k is geometry-independent, while n depends on the geometry under consideration.

Analyses have been carried out for values of d where n is an integer and for values of d where n is not an integer. In Fig. 6, results of both types have been plotted; taking $d = 0.8$ mm or $d = 0.7$ mm leads to a noninteger value of n, while taking $d = 0.778$ mm and $d = 0.689$ mm leads to $n = 7$ and $n = 8$, respectively. It can be verified that the number of wave lengths along the bar as given by the numerically obtained strain profiles corresponds perfectly to the value of n as given by Eq. (22) or Fig. 5. For the two analyses where n is not an integer (Fig. 6, left

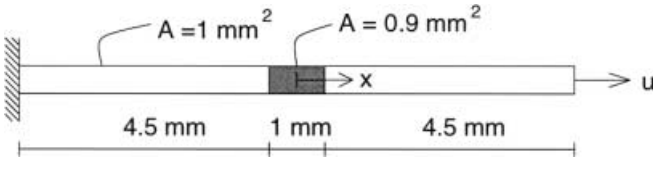

Fig. 4. Bar: problem statement for static analysis

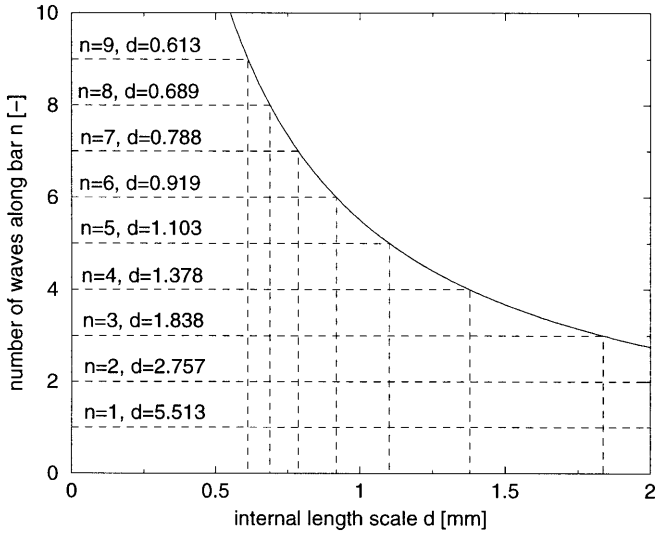

Fig. 5. Relation between the number of wave lengths along the bar n and the internal length scale d of the second-gradient model for the bar problem with $L = 10$ mm

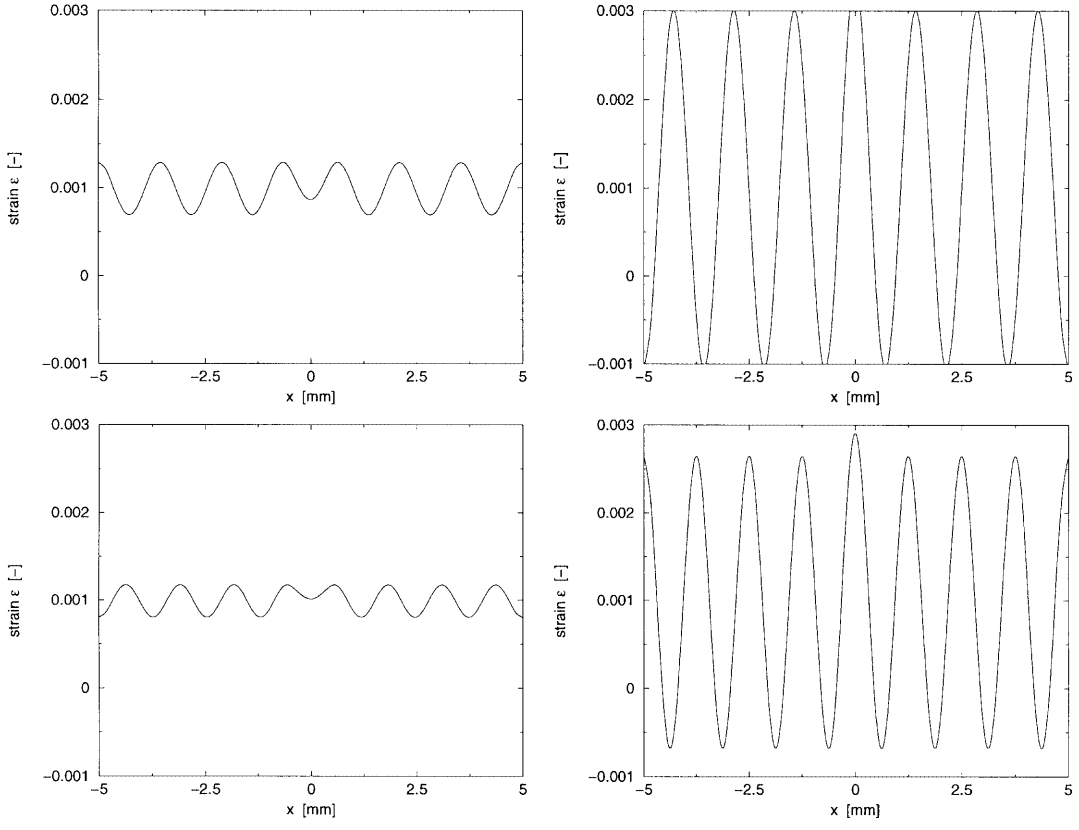

Fig. 6. Bar: static response of the second-gradient model with positive sign, strain profiles for $d = 0.8$ mm (top left), $d = 0.788$ mm (top right), $d = 0.7$ mm (bottom left) and $d = 0.689$ mm (bottom right)

column), uniqueness is guaranteed; as such, moderate oscillations in the strain profile are obtained. In contrast, when n is an integer (Fig. 6, right column) the solution is nonunique, which becomes manifest by the extreme oscillations in the strain profile. In fact, the analytical solution for the cases that n is an integer is undetermined, causing the numerical solution to be arbitrarily dependent on round-off errors and discretisation aspects. In short, the static analysis shows that the results should be distrusted for a limited number of values for the internal length scale d. However, it remains an undesirable feature of this model that a local perturbation, as given by the imperfection in Fig. 4, leads to strain oscillations in the complete domain.

5.2
Second-gradient model with negative sign

Next, the second-gradient model with the negative sign, Eq. (1), is used to analyse the problem of Fig. 4. As has been mentioned in Sec. 2, the analytical solution has an exponential character. No instabilities are to be expected, and uniqueness is guaranteed. Fig. 7 shows the response of this model for values of the internal length scale $d = 0.5$ mm and $d = 1$ mm. Although the cross-sectional area is discontinuous over the bar length, the strain profile along the bar is smooth due to the higher-order strain gradients that are present in the constitutive relation. This smoothing effect becomes more pronounced for larger values of the internal length scale d. Furthermore, local perturbations remain local. Thus, the second-gradient model with the negative sign yields physically realistic results.

5.3
Fourth-gradient model

Finally, the performance of the fourth-gradient model is tested for the bar problem of Fig. 4. A general analytical expression for the displacement field in the bar can be derived as (see Appendix B)

$$u = C_1 + C_2 x + \exp\left(\frac{-\tau_1 x}{d}\right)\left[C_3 \cos\left(\frac{\tau_2 x}{d}\right) + C_4 \sin\left(\frac{\tau_2 x}{d}\right)\right] + \exp\left(\frac{\tau_1 x}{d}\right)\left[C_5 \cos\left(\frac{\tau_2 x}{d}\right) + C_6 \sin\left(\frac{\tau_2 x}{d}\right)\right] , \tag{23}$$

where C_i are constants that have to be determined according to the boundary conditions. Furthermore, $\tau_1 = \sqrt{\sqrt{90} - 15/2}$ and $\tau_2 = \sqrt{\sqrt{90} + 15/2}$ are model-specific coefficients, which follow from the factors 1/12 and 1/360 that precede the second-gradient and fourth-gradient terms in the constitutive relation Eq. (16). From Eq. (23), it can be seen that the harmonic terms of the solution are multiplied with exponential terms. This implies that local perturbations of the strain field can remain local, which is in contrast to the response of the second-gradient model with the positive sign.

The coefficient of the harmonic terms in Eq. (23) equals τ_2/d. In the second-gradient model with the positive sign, the wave number has been found as $k = \sqrt{12}/d$ in the argument of the harmonic terms of the analytical solutions. With these considerations, for the fourth-gradient model, the number of wave lengths along the bar can be found by replacing the factor $\sqrt{12}$ in Eq. (22) by the factor τ_2. Thus,

$$n = \frac{L\sqrt{\sqrt{90} + \frac{15}{2}}}{2\pi d} . \tag{24}$$

Again, d can be selected such that n equals an integer. However, in contrast to the second-gradient model, no anomalies are expected from the point of view of uniqueness, energy considerations or dispersion analysis when n is an integer.

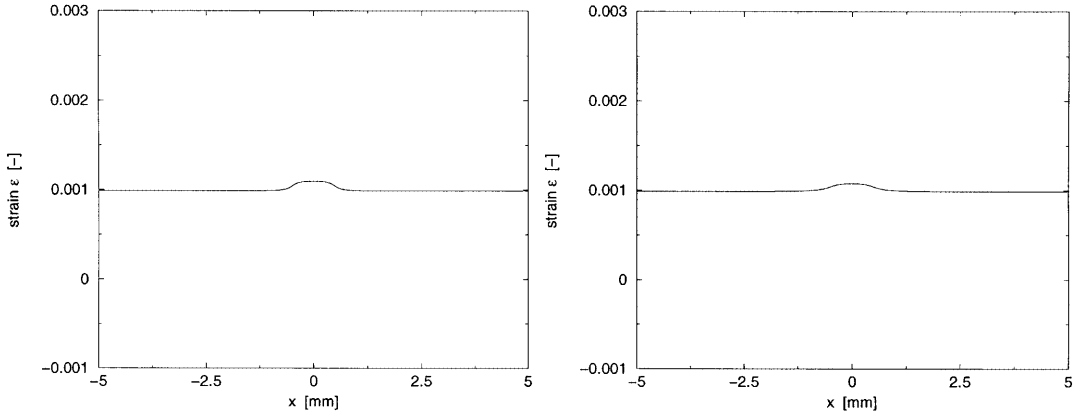

Fig. 7. Bar: static response of the second-gradient model with negative sign, strain profiles for $d = 0.5$ mm (left) and $d = 1$ mm (right)

Four numerical analyses have been carried out, two with a value for the internal length scale d where n is an integer, and two with a value for d where n is not an integer. In Fig. 8, the strain profiles plotted for the cases $d = 0.8$ mm, $d = 0.729$ mm (which corresponds to $n = 9$), $d = 0.7$ mm and $d = 0.656$ mm (which corresponds to $n = 10$). The four results show very little differences. Indeed, instabilities are absent in the fourth-gradient model. Another important observation is that local perturbations of the strain field remain local and do not extend over the entire domain, which is physically realistic.

6
Linear dynamic analysis

The problem statement for the dynamic analysis is given in Fig. 9. A Heaviside loading function is applied so that a shock wave propagates through the bar. The force amplitude is $F_0 = 5$ N, the Young's modulus is taken as $E = 1000$ MPa, and the mass density is $\rho = 1000$ N s^2/mm^4. For the spatial discretisation, the EFG method is used. Again, 81 equally-spaced nodes and 400 equally-spaced integration points have been used. For the time discretisation, the implicit Newmark scheme is used, [14, 25], with the time step $\Delta t = 0.2$ s and the Newmark parameters $\gamma = 0.5$ and $\beta = 0.25$ (average acceleration method), unless mentioned otherwise. Although not shown here, similar results have been found for smaller time steps.

6.1
Second-gradient model with positive sign

Firstly, the second-gradient model with the positive sign is taken to model the problem of Fig. 9. In the problem under consideration, in which a shock wave is generated, all harmonics are present in the response. As can be seen from Fig. 3, this implies that wave numbers with real frequencies (lower wave numbers) as well as wave numbers with imaginary frequencies (higher wave numbers) are triggered by the loading conditions. While real angular frequencies represent waves with a finite propagation speed, imaginary angular frequencies denote waves that propagate instantaneously everywhere in the domain. This is illustrated in Fig. 10, in which the

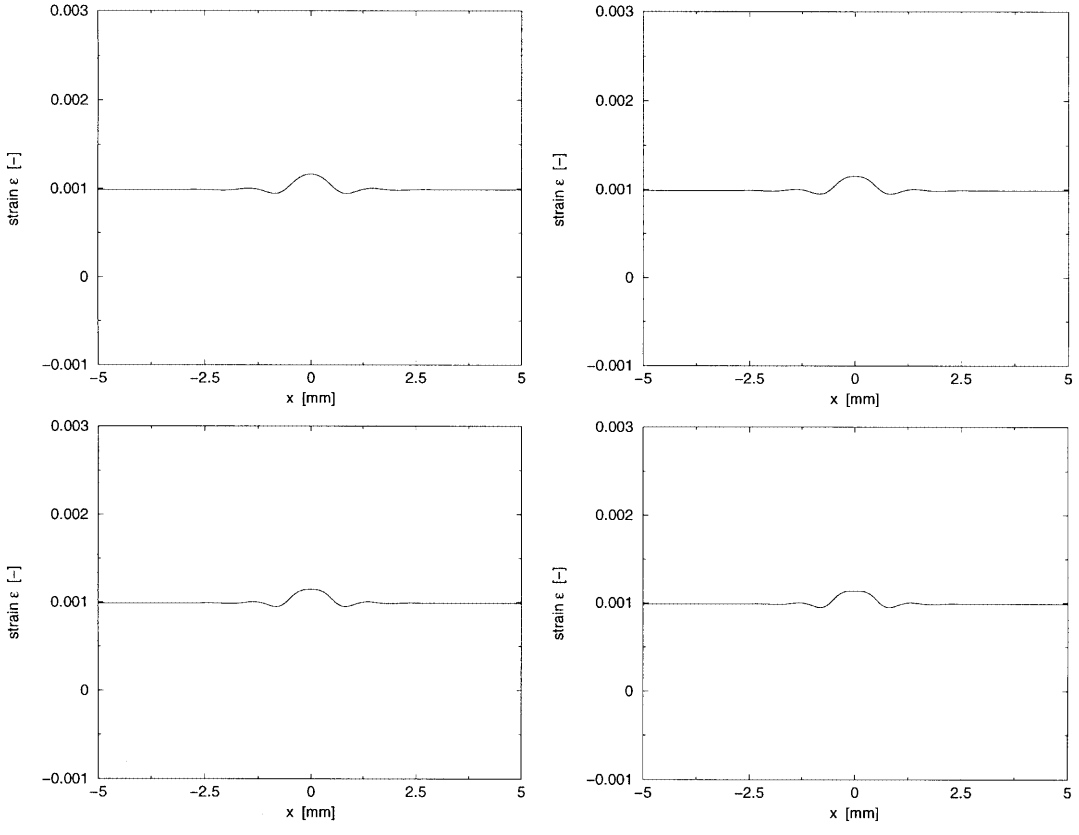

Fig. 8. Bar: static response of the fourth-gradient model, strain profiles for $d = 0.8$ mm (top left), $d = 0.729$ mm (top right), $d = 0.7$ mm (bottom left) and $d = 0.656$ mm (bottom right)

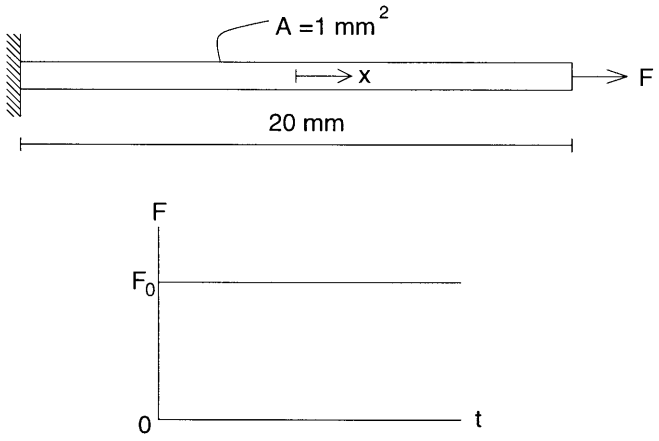

Fig. 9. Bar: problem statement for dynamic analysis, geometry and loading conditions (top) and load-time diagram (bottom)

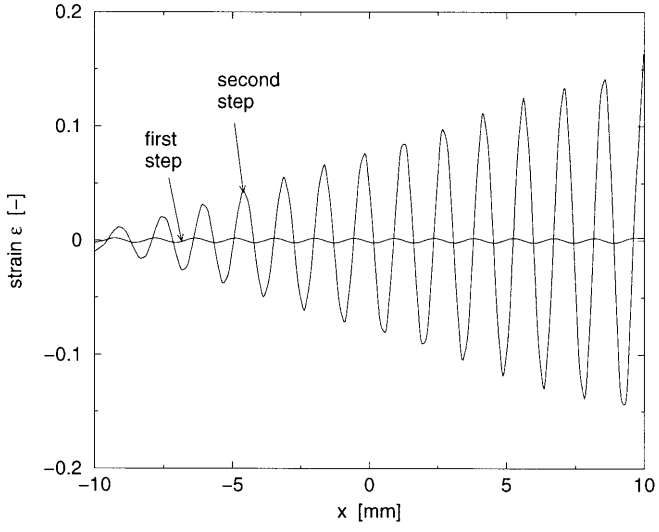

Fig. 10. Bar: dynamic response of the second-gradient model with positive sign, strain profiles for first two time steps

dynamic response of the second-gradient model is plotted for the problem of Fig. 9. The internal length scale is $d = 2$ mm. Only the strain profiles corresponding to the first two time increments are plotted. It can be seen that after the first time increment the influence of the shock wave is present in the entire bar, which is unrealistic. After the second time increment, the amplitude of the strain profile increases in an unphysical manner to unrealistically large values. In the classical continuum, the strain profile would have propagated only marginally, while the amplitude would have remained bounded.

As such, the second-gradient model with a positive sign is unsuitable for numerical dynamic analyses. While the model instabilities in *statics* are restricted to specific choices for n (Eq. (22)), the use of this model in *dynamics* leads to anomalies for any loading condition that triggers wave numbers larger than the critical value $\sqrt{12}/d$.

6.2
Second-gradient model with negative sign

Next, the second-gradient model with the negative sign has been used to simulate the problem of Fig. 9. As has been noted in Fig. 3, in this model no imaginary angular frequencies occur. However, all wave lengths are associated with phase velocities that are higher than that of the classical continuum.

In Fig. 11, the strain profiles at time $t = 4$ s, $t = 8$ s, $t = 12$ s and $t = 16$ s are plotted. A range of values for the internal length scale d has been taken, including the case of the classical continuum $d = 0$ mm. For $d > 0$, it can be seen that the shape of the front changes with increasing time, which illustrates the dispersive character of the medium. This dispersive effect is the result of the inclusion of higher-order gradients; in a classical continuum (the case with $d = 0$ mm in Fig. 11) the shape of the front remains unaltered in time (neglecting numerical dispersion effects). For larger values of d, the dispersion becomes more significant. Another observation is that, for finite values of d, the front of the wave propagates faster than for the case $d = 0$, which is consistent with the dispersion analysis in Sec 4. This unrealistically fast propagation speed of the wave front is a disadvantage of this model.

6.3
Fourth-gradient model

Finally, the fourth-gradient model is used for modelling the problem in Fig. 9. In contrast to the second-gradient model with a positive sign, no wave numbers with imaginary angular frequencies exist, as can be verified from Fig. 3. Thus, the numerical deficiencies as they have appeared for the second-gradient model with a positive sign are not to be expected for the fourth-gradient model.

In Fig. 12, the propagation of the strain profile is plotted for a range of internal length scales d, and at time $t = 4$ s, $t = 8$ s, $t = 12$ s and $t = 16$ s. In comparison with the response of the second-gradient model with the positive sign, in the fourth-gradient model the strain profile propagates in a realistic manner for all values of d. The propagation speed is finite, and the amplitude of the strain profile remains bounded. It can be seen that, depending on the value of d, the front of the wave changes in shape during the propagation. For higher values of d, the dispersive character of the model becomes more pronounced.

A peculiar phenomenon that occurs in all analyses with $d > 0$ is the appearance of high-frequent waves that propagate *ahead of* the actual front of the strain profile. The existence of these high-frequent waves can be understood from the fact that (i) all frequencies are triggered

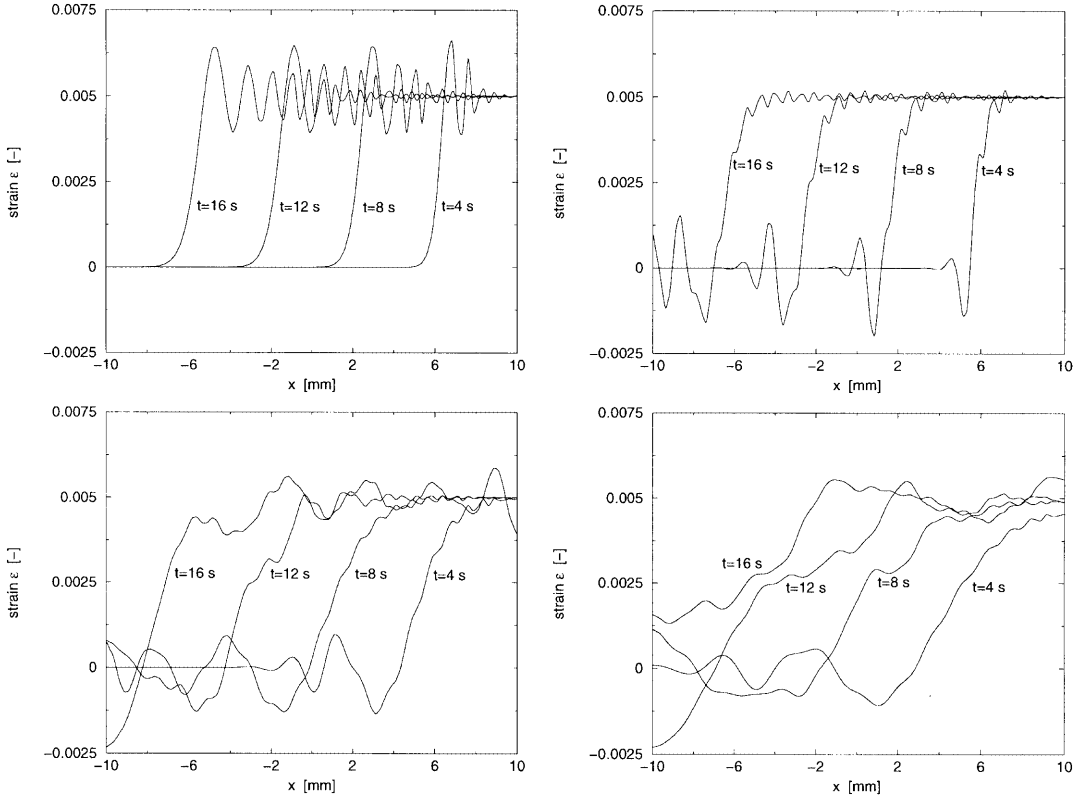

Fig. 11. Bar: dynamic response of the second-gradient model with negative sign, propagation of the strain profile for $d = 0$ mm (top left), $d = 0.5$ mm (top right), $d = 2$ mm (bottom left) and $d = 5$ mm (bottom right)

by the current shock-wave loading conditions, and (ii) in the present fourth-gradient model, the higher wave numbers are associated with phase velocities that are larger than the bar velocity $\sqrt{E/\rho}$ (see Fig. 3). In contrast, in the response of the second-gradient model with the negative sign, *all* wave numbers have a phase velocity larger than the bar velocity, causing the propagation speed of the complete wave front to be unrealistically high.

Damping of the artificial high-frequency fast-propagating waves can be attained in various ways. For instance, the Newmark parameter γ can be increased, [14, 26]. In Fig. 13, the propagating strain profile is plotted again for the case $d = 2$ mm, but now with $\gamma = 0.7$ and $\beta = (\gamma + 1/2)^2/4 = 0.36$. Indeed, numerical damping of the high frequencies is obtained, although a high-frequency wave propagating faster than the wave front still appears. Alternatively, the combination of an implicit time integration scheme with a lumped mass matrix may be considered to increase numerical damping, [26], although this option is not considered here. In any case, the magnitude of this artificial high-frequency wave decreases for increasing

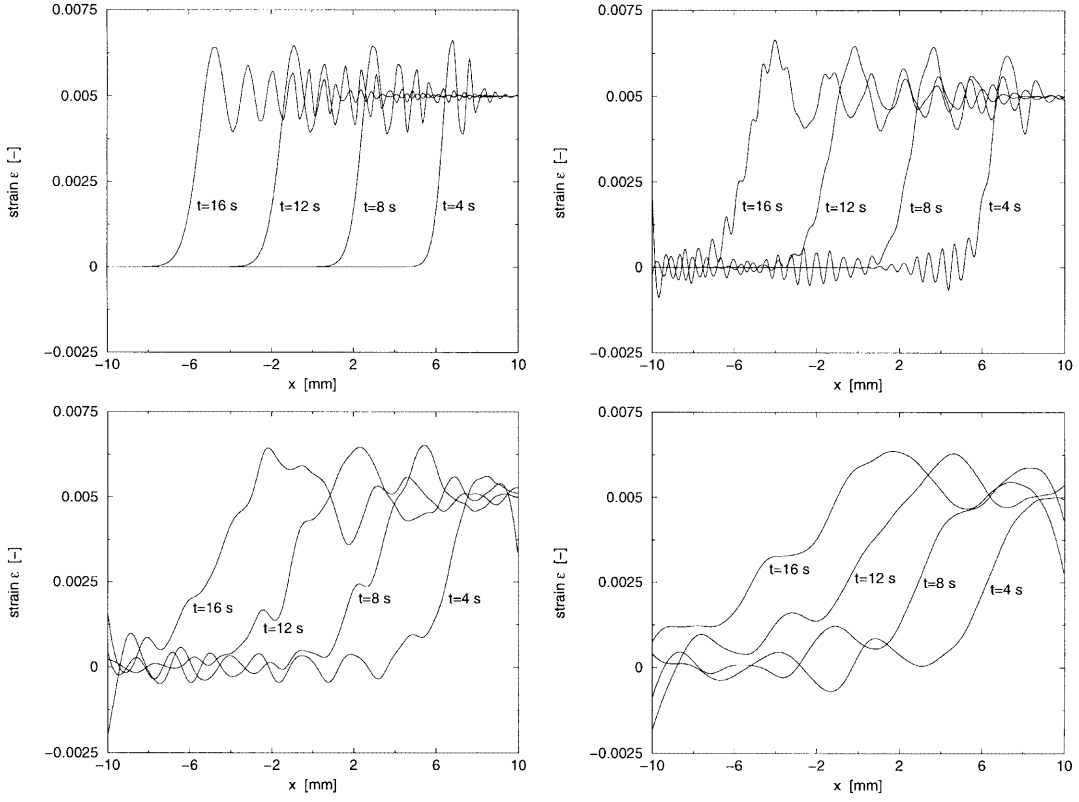

Fig. 12. Bar: dynamic response of the fourth-gradient model, propagation of the strain profile for $d = 0$ mm (top left), $d = 0.5$ mm (top right), $d = 2$ mm (bottom left) and $d = 5$ mm (bottom right)

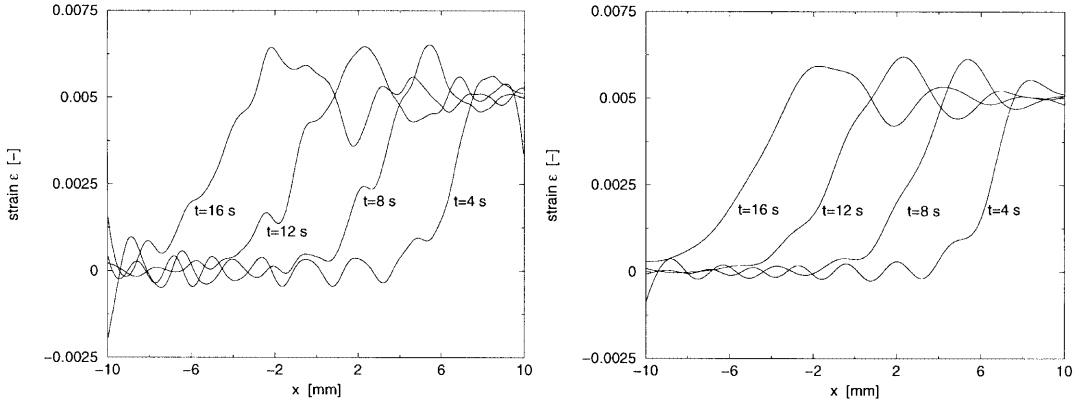

Fig. 13. Bar: dynamic response of the fourth-gradient model with $d = 2$ mm; influence of Newmark parameters: $\gamma = 0.5$ and $\beta = 0.25$ (left), $\gamma = 0.7$ and $\beta = 0.36$ (right)

time, so that eventually its influence will become negligible. Furthermore, it must be realised that the discretisation sets an upper bound to the wave numbers that can be transmitted; the infinitely high wave numbers that would travel with an infinitely high velocity can never be captured by a finite discretisation fineness.

7
Conclusions

In this paper, several types of strain-gradient models are studied. A distinction is made between two motivations for the incorporation of higher-order strain gradients into a classical continuum: firstly, regularisation or smoothing of singularities or discontinuities in the strain field, and, secondly, the introduction of heterogeneity. In both cases, an internal length scale related to the size of the microstructure enters the model. A typical second-order strain-gradient model of either case is studied analytically, where it has been found that the sign of the second-order gradient term drives the uniqueness and the stability of the model. A second-gradient model with a negative sign, as is classically used to regularise singularities, guarantees uniqueness and stability, but lacks a direct link with the underlying microstructure. On the other hand, a second-gradient model with positive sign can be derived directly from a discrete medium, but the model can become unstable and uniqueness is not guaranteed.

To combine the advantageous properties of the two types of second-gradient models, a fourth-order strain-gradient model is derived from a discrete medium. It is demonstrated that this fourth-gradient model is unconditionally stable, while the link with the underlying microstructure is evident.

Linear static and dynamic numerical analyses have been carried out to assess the performance of the higher-order gradient models. The element-free Galerkin method has been used, since this method facilitates the incorporation of higher-order strain gradients.

The static response of the second-gradient model with a positive sign is found to be unstable for a selected number of values of the internal length scale. In other cases, a stable response is found, although local perturbations lead to oscillations in the entire domain. The responses of the second-gradient model with a negative sign and of the fourth-gradient model in statics are physically realistic and mathematically sound: no instabilities are found, and local perturbations remain local.

In dynamics, the differences between the models become more pronounced. The second-gradient model with positive sign fails completely due to imaginary propagation velocities of the higher wave numbers. These higher wave numbers are especially dominant when shock waves are generated. Thus, this second-gradient model is not suitable to study practical dynamic problems. The second-gradient model with negative sign gives stable results, but all waves propagate with a velocity that is unrealistically high (i.e. higher than the bar velocity of the classical continuum). On the other hand, in the fourth-gradient model, all propagation velocities are real, and realistic responses are found. The model shows a dispersive character, and the intensity of the dispersion depends on the internal length scale parameter. However, waves are found that propagate with an unrealistically high velocity, but this only concerns the higher wave numbers, and their influence on the global response appears to be limited in the presented analysis.

Appendix A
Discretisation aspects

Below, the discretised system of equations will be derived that has been used to perform the EFG analysis with the higher-order gradient continua in Secs. 5 and 6. Starting point is the weak format of the one-dimensional equation of the motion, i.e.

$$\int_0^L \delta u \rho \ddot{u} \mathrm{d}x = \int_0^L \delta u \frac{\partial \sigma}{\partial x} \mathrm{d}x \ , \tag{25}$$

in which body forces are left out of consideration. The general constitutive equation is written as

$$\sigma = E(\varepsilon + c_1 \nabla^2 \varepsilon + c_2 \nabla^4 \varepsilon) \ , \tag{26}$$

where $(c_1, c_2) = (\frac{1}{12}d^2, 0)$ for the second-gradient model with a positive sign, $(c_1, c_2) = (-\frac{1}{12}d^2, 0)$ for the second-gradient model with negative sign, and $(c_1, c_2) = (\frac{1}{12}d^2, \frac{1}{360}d^4)$ for the fourth-gradient model. Equation (26) is substituted into Eq. (25), the kinematic relation $\varepsilon = \partial u/\partial x$ is used, and the higher-order terms are integrated by parts. Thus,

$$\int_0^L \delta u \rho \ddot{u} \mathrm{d}x + \int_0^L \frac{\partial \delta u}{\partial x} E \frac{\partial u}{\partial x} \mathrm{d}x - \int_0^L \frac{\partial^2 \delta u}{\partial x^2} E c_1 \frac{\partial^2 u}{\partial x^2} \mathrm{d}x$$

$$+ \int_0^L \frac{\partial^3 \delta u}{\partial x^3} E c_2 \frac{\partial^3 u}{\partial x^3} \mathrm{d}x = \left[\delta u E(\varepsilon + c_1 \nabla^2 \varepsilon + c_2 \nabla^4 \varepsilon)\right]_0^L - \left[\frac{\partial \delta u}{\partial x} E c_2 \frac{\partial^4 u}{\partial x^4}\right]_0^L \quad . \tag{27}$$

The first boundary term in the right-hand-side of Eq. (27) can be identified as the conventional traction boundary term. The second boundary term cancels by assuming vanishing fourth-order derivatives of the displacement, [6]. The first two domain integrals in the left-hand-side of Eq. (27) concern with the conventional mass matrix and stiffness matrix, respectively. The third and fourth domain integral represent the higher-order contributions of the models. After discretisation, a global system of equations is obtained as

$$\mathbf{M}\ddot{\mathbf{u}} + [\mathbf{K}_0 + \mathbf{K}_1 + \mathbf{K}_2]\mathbf{u} = \mathbf{f} \quad , \tag{28}$$

where $\mathbf{u}$ contains the discretised displacements. Furthermore,

$$\mathbf{M} = \int_0^L \rho \phi_u \phi_u^T \mathrm{d}x \quad , \tag{29}$$

$$\mathbf{K}_0 = \int_0^L E \frac{\partial \phi_u}{\partial x} \frac{\partial \phi_u^T}{\partial x} \mathrm{d}x \quad , \tag{30}$$

$$\mathbf{K}_1 = -\int_0^L E c_1 \frac{\partial^2 \phi_u}{\partial x^2} \frac{\partial^2 \phi_u^T}{\partial x^2} \mathrm{d}x \quad , \tag{31}$$

$$\mathbf{K}_2 = \int_0^L E c_2 \frac{\partial^3 \phi_u}{\partial x^3} \frac{\partial^3 \phi_u^T}{\partial x^3} \mathrm{d}x \quad , \tag{32}$$

$$\mathbf{f} = [\phi_u \hat{\mathbf{t}}]_{\Gamma_n} \quad , \tag{33}$$

where $\hat{t}$ are the prescribed tractions on the boundary Γ_n.

Remark 4. Each subsequent derivative of an EFG shape function has a more oscillatory character than the previous one. To avoid zero-energy modes, the order of integration should be increased in correspondence with the *highest* derivative of the shape functions that appears in the formulation.

Appendix B
Displacement field of fourth-order model

To determine the displacement field of the fourth-order model, a general expression for the displacement $u = \exp(\mathrm{i}kx)$ is substituted in the homogeneous equilibrium equation

$$\frac{\partial^2 u(x)}{\partial x^2} + \frac{1}{12} d^2 \frac{\partial^2 u(x)}{\partial x^4} + \frac{1}{360} d^4 \frac{\partial^6 u(x)}{\partial x^6} = 0 \quad . \tag{34}$$

This leads to

$$k^2 = 0 \quad \bigvee \quad \frac{1}{360}(dk)^4 - \frac{1}{12}(dk)^2 + 1 = 0 \ . \tag{35}$$

The case $k^2 = 0$ leads to the displacement field of the classical continuum. The higher-order contribution is given through four values for dk as

$$dk = \pm\sqrt{15 \pm \mathrm{i}3\sqrt{15}} \ . \tag{36}$$

The square root of a general complex number $a + ib$ is rewritten via

$$\sqrt{a + \mathrm{i}b} = \sqrt[4]{a^2 + b^2}\exp\left(\frac{\mathrm{i}\arctan(b/a)}{2}\right) \ . \tag{37}$$

Furthermore, the following goniometric relations are used.

$$\cos\left(\frac{\arctan(b/a)}{2}\right) = \pm\sqrt{\frac{1 + \cos(\arctan(b/a))}{2}} = \pm\sqrt{\frac{1}{2} + \frac{a}{2\sqrt{a^2 + b^2}}} \ , \tag{38}$$

$$\sin\left(\frac{\arctan(b/a)}{2}\right) = \pm\sqrt{\frac{1 - \cos(\arctan(b/a))}{2}} = \pm\sqrt{\frac{1}{2} - \frac{a}{2\sqrt{a^2 + b^2}}} \ , \tag{39}$$

With these substitutions, Eq. (36) is rewritten as

$$dk = \pm\mathrm{i}\sqrt{\sqrt{90} - 15/2} \pm \sqrt{\sqrt{90} + 15/2} \ . \tag{40}$$

Introducing $\tau_1 = \sqrt{\sqrt{90} - 15/2}$ and $\tau_2 = \sqrt{\sqrt{90} + 15/2}$, and eliminating the imaginary parts of the solution, the total homogeneous solution of Eq. (34) is found as

$$\begin{aligned} u = {} & C_1 + C_2 x + \exp\left(\frac{-\tau_1 x}{d}\right)\left[C_3\cos\left(\frac{\tau_2 x}{d}\right) + C_4\sin\left(\frac{\tau_2 x}{d}\right)\right] \\ & + \exp\left(\frac{\tau_1 x}{d}\right)\left[C_5\cos\left(\frac{\tau_2 x}{d}\right) + C_6\sin\left(\frac{\tau_2 x}{d}\right)\right] \ . \end{aligned} \tag{41}$$

References

1. **Aifantis, E.C.:** The physics of plastic deformation. Int J Plasticity 3 (1987) 211–247
2. **Aifantis, E.C.:** Gradient deformation models at nano, micro, and macro scales. ASME J Eng Mat Tech 121 (1999) 189–202
3. **Aifantis, E.C.:** Strain gradient interpretation of size effect. Int J Fracture 95 (1999) 299–314
4. **Altan, B.S.; Aifantis E.C.:** On some aspects in the special theory of gradient elasticity. J Mech Behavior Mat 8 (1997) 231–282
5. **Askes, H.:** Advanced spatial discretisation strategies for localised failure – mesh adaptivity and meshless methods. Dissertation, Delft University of Technology, 2000
6. **Askes, H.; Pamin, J.; de Borst, R.:** Dispersion analysis and element-free Galerkin solutions of second and fourth-order gradient-enhanced damage models. Int J Numer Methods Eng 49 (2000) 811–832
7. **Askes, H.; Suiker, A.S.J.; Sluys, L.J.:** Dispersion analysis and element-free Galerkin simulations of higher-order strain gradient models. Mat Phys Mech 3 (2001) 12–20. Also available at http://www.ipme.ru
8. **Belytschko, T.; Krongauz, Y.; Organ, D.; Fleming, M.; Krysl, P.:** Meshless methods: an overiew and recent developments. Computer Meth Appl Mech Eng 139 (1996) 3–47
9. **Belytschko, T.; Lu, Y. Y.; Gu, L.:** Element-free Galerkin methods. Int J Numer Meth Eng 37 (1994) 229–256
10. **Chang, C.S.; Gao, J.:** Second-gradient constitutive theory for granular material with random packing structure. Int J Solids Struct 32 (1995) 2279–2293
11. **Comi, C.; Driemeier, L.:** On gradient regularization for numerical analysis in the presence of damage. In: de Borst R., van der Giessen E. (eds) Material Instabilities in Solids, Chap. 26, pp. 425–440. Amsterdam: Wiley 1998

12. **de Borst, R.; Mühlhaus, H.-B.:** Gradient-dependent plasticity: formulation and algorithmic aspects. Int J Numer Meth Eng 35 (1992) 521–539
13. **Geers, M.G.D.:** Experimental analysis and computational modelling of damage and fracture. Dissertation, Eindhoven University of Technology, 1997
14. **Hughes, T.J.R.:** The Finite Element Method – Linear Static and Dynamic Finite Element Analysis. London: Prentice-Hall 1987
15. **Jirásek, M.:** Element-free Galerkin method applied to strain-softening materials. In: de Borst R., Bićanić N., Mang H., Meschke G. (eds) Computational Modelling of Concrete Structures, pp. 311–319. Rotterdam: Balkema 1998
16. **Lasry, D.; Belytschko, T.:** Localization limiters in transient problems. Int J Solids Struct 24 (1988) 581–597
17. **Mühlhaus, H.-B.; Aifantis, E.C.:** A variational principle for gradient plasticity. Int J Solids Struct 28 (1991) 845–857
18. **Mühlhaus, H.-B.; Oka, F.:** Dispersion and wave propagation in discrete and continuous models for granular materials. Int J Solids Struct 33 (1996) 2841–2858
19. **Pamin, J.:** Gradient-dependent plasticity in numerical simulation of localization phenomena. Dissertation, Delft University of Technology, 1994
20. **Pamin, J.; Askes, H.; de Borst, R.:** An element-free Galerkin method for gradient plasticity. In: Wunderlich W. (ed) European Conference on Computational Mechanics – Solids, Structures and Coupled Problems in Engineering, TU München, 1999
21. **Peerlings, R.H.J.:** Enhanced damage modelling for fracture and fatigue. Dissertation, Eindhoven University of Technology, 1999
22. **Peerlings, R.H.J.; de Borst, R.; Brekelmans, W.A.M.; de Vree, J.H.P.:** Gradient enhanced damage for quasi-brittle materials. Int J Numerical Meth Eng 39 (1996) 3391–3403
23. **Peerlings, R.H.J.; de Borst, R.; Brekelmans, W.A.M.; de Vree, J.H.P.; Spee, I.:** Some observations on localisation in non-local and gradient damage models. Eur J Mech A/Solids 15 (1996) 937–953
24. **Schreyer, H.L.; Chen, Z.:** One-dimensional softening with localization. ASME J Appl Mech 53 (1986) 791–797
25. **Sluys, L.J.:** Wave propagation, localisation and dispersion in softening solids. Dissertation, Delft University of Technology, 1992
26. **Sluys, L.J.; Cauvern, M.; de Borst, R.:** Discretization influence in strain-softening problems. Eng Comput 12 (1995) 209–228
27. **Suiker, A.S.J.; Askes, H.; Sluys, L.J.:** Micro-mechanically based 1-D gradient damage models. In: Oñate E., Bugeda G., Suárez B. (eds) European Congress on Computational Methods in Applied Sciences and Engineering, Barcelona: CIMNE, 2000
28. **Suiker, A.S.J.; de Borst, R.; Chang, C.S.:** Micro-mechanically based higher-order continuum models for granular materials. In: Kolymbas D. (ed) Constitutive Modelling of Granular Materials, pp. 249–274. Heidelberg: Springer-Verlag, 2000
29. **Suiker, A.S.J.; de Borst, R.; Chang, C.S.:** Micro-mechanical modelling of granular material. Part 1: derivation of a second-gradient micro-polar constitutive theory. Acta Mech 149 (2001) 161–180
30. **Suiker, A.S.J.; de Borst, R.; Chang, C.S.:** Micro-mechanical modelling of granular material. Part 2: plane wave propagation in infinite media. Acta Mech 149 (2001) 181–200
31. **Triantafyllidis, N.; Aifantis, E.C.:** A gradient approach to localization of deformation. I. Hyperelastic materials. J Elas 16 (1986) 225–237
32. **Triantafyllidis, N.; Bardenhagen, S.:** On higher gradient continuum theories in 1-D non-linear elasticity. Derivation from and comparison to corresponding discrete models. J Elas 33 (1993) 259–293
33. **Vardoulakis, I.; Exadaktylos, G.; Aifantis, E.C.:** Gradient elasticity with surface energy: mode-III crack problem. Int J Solids Struct 33 (1996) 4531–4559